Response of protonated, adduct, and fragmented ions in Vocus proton-transfer-reaction time-of-flight mass spectrometer (PTR-ToF-MS)

Fangbing Li[1], Dan Dan Huang[2], Linhui Tian[1], Bin Yuan[3], Wen Tan[4], Liang Zhu[4], Penglin Ye[5], Douglas Worsnop[5], Ka In Hoi[1], Kai Meng Mok[1], Yong Jie Li[1]

[1]Department of Civil and Environmental Engineering, Department of Ocean Science and Technology, and Centre for Regional Oceans, Faculty of Science and Technology, University of Macau, Macau, China
[2]State Environmental Protection Key Laboratory of Cause and Prevention of Urban Air Pollution Complex, Shanghai Academy of Environmental Sciences, Shanghai, China
[3]Institute for Environment and Climate Research, Jinan University, Guangzhou 510632, China
[4]Tofwerk AG, Nanjing, China
[5]Aerodyne Research, Inc., Billerica, Massachusetts 01821, United States

Correspondence to: Yong Jie Li (yongjieli@um.edu.mo)

Abstract

Volatile organic compounds (VOCs) affect secondary pollutant formation via active chemistry. Proton-transfer-reaction mass spectrometry (PTR-MS) is one of the most important techniques to study the highly variable spatial and temporal characteristics of VOCs. The response of protonated, adduct, and fragmented ions in PTR-MS in changing instrument settings and varying relative humidity (RH) requires rigorous characterization. Herein, dedicatedly designed laboratory experiments were conducted to investigate the response of these ions for 21 VOCs, including 12 oxygenated VOCs and two nitriles, using the recently developed Vocus PTR-MS. Our results show that the focusing ion-molecule reactor (FIMR) axial voltage increases sensitivity by three to four orders of magnitude but does not significantly change the fractions of protonated ions. Reducing the FIMR pressure, however, substantially increases fragmentation. Applying a high radio frequency (RF) amplitude radially on FIMR can enhance sensitivity by one to two orders of magnitude without affecting the protonated ion fractions. The change in big segmented quadrupole (BSQ) amplitude mainly affects sensitivity and protonated ion fraction by modifying ion transmission. The relationship between sensitivity and proton-transfer reaction rate constant is complicated by the influences from both ion transmission and protonated ion fraction. The protonated ions of most VOCs studied (19 out of 21) show less than 15% variations in sensitivity as RH increases from ~5% to ~85%, except for some long-chain aldehydes which show a positive RH variation of up to 30%. Our results suggest that the Vocus PTR-MS can reliably quantify the majority of VOCs under ambient conditions with varying RH. However, caution is advised for small oxygenates such as formaldehyde and methanol due to their low sensitivity, as well as for long-chain aldehydes for their slight RH dependence and fragmentation.

1 Introduction

Atmospheric volatile organic compounds (VOCs) affect atmospheric chemistry by forming secondary pollutants such as tropospheric O_3 (Shao et al., 2016) and secondary organic aerosols (SOA) (Shrivastava et al., 2017). In addition to their low mixing ratios (parts per billion by volume, ppbv, or even lower), the spatial and temporal variabilities of atmospheric VOCs pose another analytical challenge to the study of their atmospheric occurrence, sources, and fates. Mass spectrometric (MS) techniques based on ion-molecule reactions (IMR) (Španěl and Smith, 1996) or specifically proton-transfer reactions (PTR) (Hansel et al., 1995;Lindinger et al., 1998) in a selected ion flow tube (SIFT) have been developed to provide fast-responding measurements of VOCs. These techniques, especially the PTR-MS, have been widely used in VOC measurements in outdoor and indoor environments (Salazar Gómez et al., 2021;Sekimoto and Koss, 2021;Pagonis et al., 2019;Pleil et al., 2019;Claflin et al., 2021;Schripp et al., 2014;Jensen et al., 2021).

Quantification of VOCs (denoted as M) by PTR-MS relies heavily on their proton-transfer reactions with the hydronium ion H_3O^+ (R1). In early SIFT-MS studies where reagent ions include a multitude of $H_3O^+(H_2O)_n$ (n =0, 1, 2, 3…) ion series (Španěl and Smith, 2000), proton-transfer reactions with more hydrated (n ≥ 1) hydronium ions (R2a) are also important for species with proton affinity (PA) larger than water clusters. In addition, ligand switching reactions (R2b) and association reactions (R3, with N being N_2 or O_2) are also common, leading to $[MH + H_2O]^+$ instead of MH^+. Under these circumstances, the quantification of VOCs might be heavily influenced by water vapor concentration, or relative humidity (RH), of the sample. For instance, acetone concentrations in exhaled air were overestimated by 13% even using both protonated (MH^+) and water adduct ($[MH + H_2O]^+$) ions for quantification, when water vapor varied in the range of $(1 - 10) \times 10^{12}$ molecules cm^{-3} (Španěl and Smith, 2000). A later study (Smith et al., 2001) showed that quantification of other oxygenated VOCs (OVOCs) such as ethyl acetate, diethyl ether, methanol, ethanol, and propanol by SIFT-MS also suffered from RH dependence to various degrees.

$$M + H_3O^+ \rightarrow MH^+ + H_2O \qquad (R1)$$

$$M + H_3O^+(H_2O)_n \rightarrow MH^+ + (H_2O)_{n+1} \qquad (R2a)$$

$$M + H_3O^+(H_2O)_n \rightarrow [MH + H_2O]^+ + (H_2O)_n \qquad \text{(R2b)}$$

$$MH^+ + H_2O + N \rightarrow [MH + H_2O]^+ + N \qquad \text{(R3)}$$
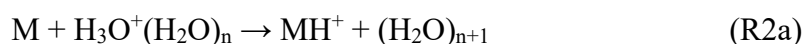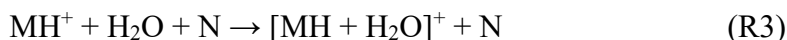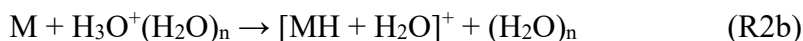
For PTR-MS that normally uses the MH^+ for quantification, RH dependence was also widely reported. For instance, Warneke et al. (2001) reported that the sensitivity of benzene in PTR-MS decreased significantly with the increase of RH, while Steinbacher et al. (2004) suggested a slight decrease with the increase of RH. Quantification of biogenic volatile organic compounds (BVOCs) was also reported to be slightly affected by RH (Kari et al., 2018). The RH dependence stems from the change of reagent ion distribution, i.e., among H_3O^+ and $H_3O^+(H_2O)_n$ ($n \geq 1$), which can lead to overestimation or underestimation of VOCs if such dependence is strong because ambient RH is deemed highly variable. Therefore, RH-dependent calibrations for VOC measurements using PTR-MS were normally recommended (de Gouw and Warneke, 2007;Inomata et al., 2008;Sinha et al., 2009;Vlasenko et al., 2010;Cui et al., 2016;Michoud et al., 2018).

Another complication in VOC measurements using SIFT-MS or PTR-MS is that, due to the nucleophilicity of the oxygen atom, protonated OVOCs would dehydrate, forming fragmented ions (R4). This reaction often occurs in heavy alcohols, aldehydes, and carboxylic acids (Španěl et al., 1997;Ŝpaněl and Smith, 1998;Hartungen et al., 2004;Baasandorj et al., 2015).

$$MH^+ \rightarrow [MH - H_2O]^+ + H_2O \qquad \text{(R4)}$$
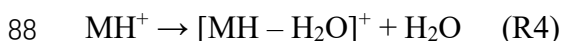
In addition, cleavage on the C-C bond of the protonated ion (R5) is also possible, especially for alkyl-substituted VOCs under high-energy conditions (e.g., a high E/N ratio, which is the reduced electric field parameter with E being the electric field and N the number density of the gas in the drift tube).

$$MH^+ \rightarrow [MH - C_xH_y]^+ + C_xH_y \qquad \text{(R5)}$$
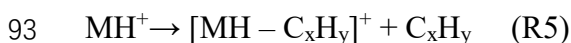
For instance, at an E/N ratio of 120 Townsend (Td), substituted monocyclic aromatic compounds such as ethylbenzene and propylbenzene start to fragment into a benzenium ion ($C_6H_7^+$) (de Gouw et al., 2003;Gueneron et al., 2015).

A newly designed focusing ion-molecule reactor (FIMR) was used for PTR-MS, termed Vocus, and has been shown to have little RH dependence for the protonated ion because of the high concentration of water vapor introduced into the FIMR (Krechmer

100 et al., 2018). The concentration of hydronium ion (H_3O^+) in the FIMR is high enough

101 to maintain at a constant level and dominate over other side reactions, thereby

102 minimizing the RH dependence for VOC measurement. Yet, the formation of adduct

103 ions and fragmented ions in Vocus PTR-MS as a function of RH has not been fully

104 scrutinized, hindering a complete understanding of the ion chemistry in the Vocus PTR-

105 MS and potential cross interference when measuring ambient air with complex VOC

106 mixtures. Herein, we conducted experiments on the effects of instrumental settings and

107 RH variations on the quantification of 21 VOCs, including 12 OVOCs and 2 nitriles,

108 using a Vocus PTR-MS. Response of protonated ions (MH^+), adduct ions ($[MH +$

109 $H_2O]^+$), and fragmented ions ($[MH – H_2O]^+$ or $[MH – C_xH_y]^+$) of these VOCs was

110 investigated as a function of instrumental setting and RH. Results are interpreted based

111 on the PA values and/or proton-transfer reaction rate constants (k_{ptr}). Some caveats on

112 using the Vocus PTR-MS to measure VOCs, especially OVOCs, are also provided.

113 **2 Methodology**

114 **2.1 Instrument settings**

115 Experiments were performed with a Vocus proton-transfer-reaction time-of-flight

116 mass spectrometer (PTR-ToF-MS, Vocus 2R, TOFWERK AG, Thun, Switzerland),

117 hereinafter referred to as Vocus. The Vocus consists of (i) a discharge ion source, (ii) a

118 focusing ion-molecule reactor (FIMR), (iii) a big segmented quadrupole (BSQ), (iv) a

119 series of direct current (DC) optics that further focus and accelerate the primary beam

120 (PB), and (v) a time-of-flight (ToF) mass analyzer (Krechmer et al., 2018). The ion

121 source is a plasma discharge composed of two conical surfaces. Water vapor is supplied

122 by purging 20 to 30 mL of milli-Q water and is ionized by plasma discharge. The

123 reagent ions pass through a ring offset from the central axis so that the photons

124 generated by the discharge cannot enter. The drift tube was improved by replacing the

125 stacked ring electrodes of the traditional PTR-MS with a FIMR, which is a glass tube

126 with a resistive coating on the inner surface and a quadrupole with a radio frequency

127 (RF) electric field applied. The FIMR increases ion transmission by a factor of 7 to 9

128 and sensitivity by more than one order of magnitude (Krechmer et al., 2018). Moreover,

129 the mean kinetic energy of H_3O^+ is increased by three times, and the formation of more

130 hydrated hydronium ions is reduced, suppressing RH dependence for most VOCs

131 measured (Krechmer et al., 2018). Meanwhile, the mean kinetic energy of VOCs

measured is not significantly increased, thereby minimizing fragmentation (Krechmer et al., 2018). The ToF mass analyzer offers a mass resolving power of 12,000 at a mass-to-charge ratio (m/Q) of 107 Thomson (Th).

In our experiments, sample air was drawn into the instrument using 0.5 m long perfluoroalkoxy (PFA) Teflon tubing of ~0.5 m length and 1/4″ outer diameter, with a flow rate of 0.5 L·min^{-1}. Most of the sample air was directed to the exhaust, while the actual flow into the FIMR was around 0.15 L·min^{-1}. In typical experiments, the FIMR was operated at a pressure of 2.0 mbar and a temperature of 373.15 K. The axial and radial voltages were normally set to be 625 and 500 V, respectively, unless stated otherwise.

We also performed experiments by varying the instrument settings such as FIMR axial voltage (V) and FIMR pressure (p), both of which affect the E/N ratio, as well as RF and BSQ amplitudes to investigate how protonated, adduct, and fragmented ions respond to those changes. These experiments were performed under dry (RH ~5%) conditions, and the concentrations were approximately 12 ppbv for most VOCs (except for β-caryophyllene at about 1.2 ppbv). The instrument settings were varied by: 1) changing the FIMR axial voltage from 260 to 700 volts, 2) changing the pressure in FIMR from 1.5 to 3.5 mbar; 3) changing the RF amplitude from 13 to 500 volts (with p of 2.0 or 3.5 mbar); 4) changing the BSQ voltage from 50 to 300 volts (with p of 2.0 or 3.5 mbar). The other instrument settings were fixed as the default values while changing the tested ones. Specifically, RF amplitude was at 500 volts and BSQ amplitude was at 300 volts when changing E (i.e., V) and N (i.e., p), and an E/N ratio of 142 Td was used when changing RF and BSQ amplitudes (Table S1).

2.2 Experimental setup

The VOCs (Table S2 and Figure 1) in mixtures from two cylinders were separately delivered to the dilution and/or RH control setup (Figure S1). Dilution air was generated from a zero-air generator (Environics series 7000, Environics Analytics Group Ltd., Canada). Gas cylinder I (Table 1, Apel-Riemer Environmental Inc., US, valid for 12 months) contains mainly hydrocarbons, while gas cylinder II (Table 1, Linde Gases, US, valid for 12 months) contains mainly OVOCs and nitriles. Most VOCs in the cylinders are at approximately 1000 ppbv, except for β-caryophyllene that is at approximately 100 ppbv. Table S2 shows their CAS numbers, m/Q values of the

164 protonated ions (MH$^+$), as well as PA and k_{ptr} values. According to their functional

165 groups, the 21 VOCs are grouped into 9 categories, and Figure 1 shows their structures.

166 Note that although n-butanal and methyl ethyl ketone are isomers, they are in different

167 cylinders and measured separately, thus will not interfere with each other.

168 Dry experiments were performed by diluting the VOCs from the cylinders with dry zero

169 air with 7 concentrations from 0 to approximately 22 ppbv (or approximately 2 ppbv

170 for β-caryophyllene). For each concentration step, measurements lasted for about half

171 an hour for gas cylinder I with hydrocarbons but about two hours for gas cylinder II

172 with OVOCs and nitriles. The 2-hour stabilization time for cylinder II, which contained

173 mainly OVOCs and nitriles, should be sufficient because even with half-an-hour

174 stabilization time for cylinder I, the overlapping species acetone and acetaldehyde

175 showed deviations of less than ±1.5% in sensitivity. Other measures such as minimizing

176 the length of the Teflon tube at the inlet (less than 30 cm) were also undertaken to allow

177 fast establishment of equilibrium-state concentrations for OVOCs. In RH-dependent

178 experiments (Figure S1), dilution was made by RH-conditioned air produced from a

179 humidity generator (OHG-4, Owlstone, US). The accuracy of the RH sensor (RH-USB

180 Probe, Omega) is within 4% of RH. Nine RH ramping steps from ~5% to ~85% with

181 approximately 10% intervals were used, and the VOCs were set with 4 concentrations

182 from 0 to approximately 12 ppbv (or approximately 1.2 ppbv for β-caryophyllene).

183 After the initial equilibration of 0.5 hours under dry conditions (RH ~5%), each RH

184 ramping lasted for 15 min. Triplicate experiments were performed for the highest

185 concentration.
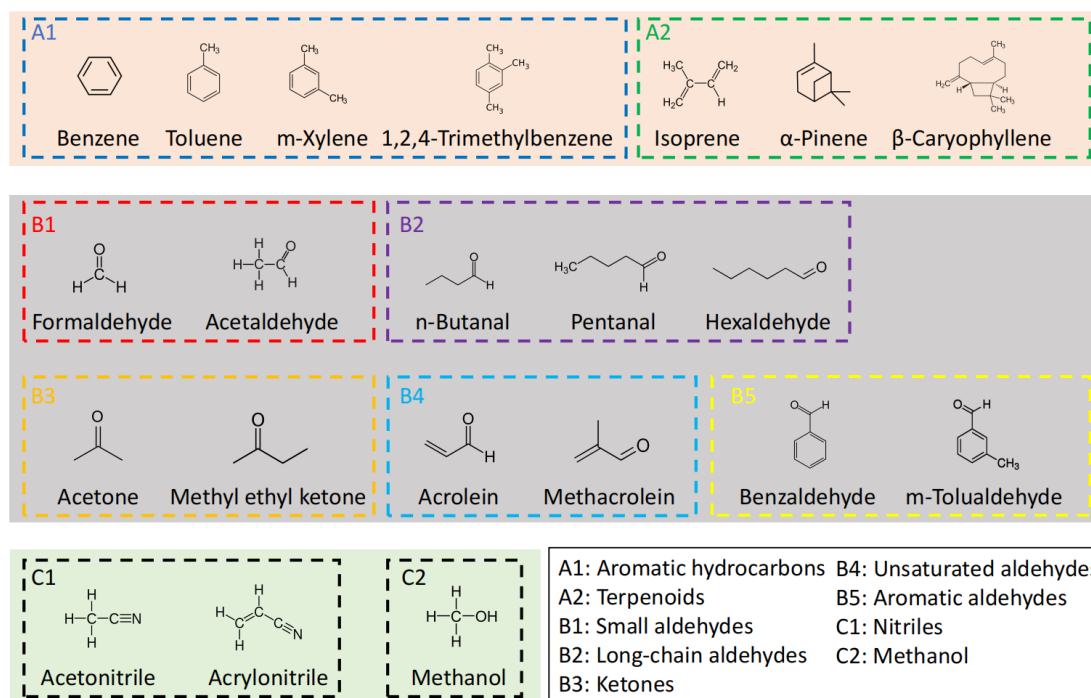
186
187 Figure 1. Names, structures, and grouping of the 21 VOCs in this study. These VOCs
188 were prepared in two gas standard cylinders (I and II) with mixing ratios of ~1000 ppbv
189 (~100 ppbv for β-caryophyllene), balanced by N_2. Acetaldehyde and acetone are
190 present in both gas standard cylinders, with concentrations differing by <5%. n-Butanal
191 and methyl ethyl ketone are isomers but are in different gas standard cylinders.

2.3 Data analysis

193   The Vocus data were analyzed with the manufacturer-supplied software package
194 Tofware (v3.2.3) based on Igor Pro (Wavemetrics). Peak fitting was performed using
195 Tofware routines and the measured m/Q values of the pronated ions (MH^+) are shown
196 in Table S2 together with their exact m/Q values. In addition to MH^+, we also looked
197 for adduct ions ($[MH + H_2O]^+$), and fragmented ions ($[MH - H_2O]^+$ or $[MH - C_xH_y]^+$),
198 since those ions are also anticipated for VOCs, especially OVOCs, in PTR-MS
199 measurements (Pagonis et al., 2019). Although the VOCs were in mixtures and showed
200 ensemble mass spectra, we constructed the mass spectrum for each VOC by plotting
201 their identified adduct or fragmented ions alongside the protonated ions, as shown in
202 Figures S2-S4 in the SI. Their percentage contributions are presented in Figure 2 and
203 numerically in Table S4.
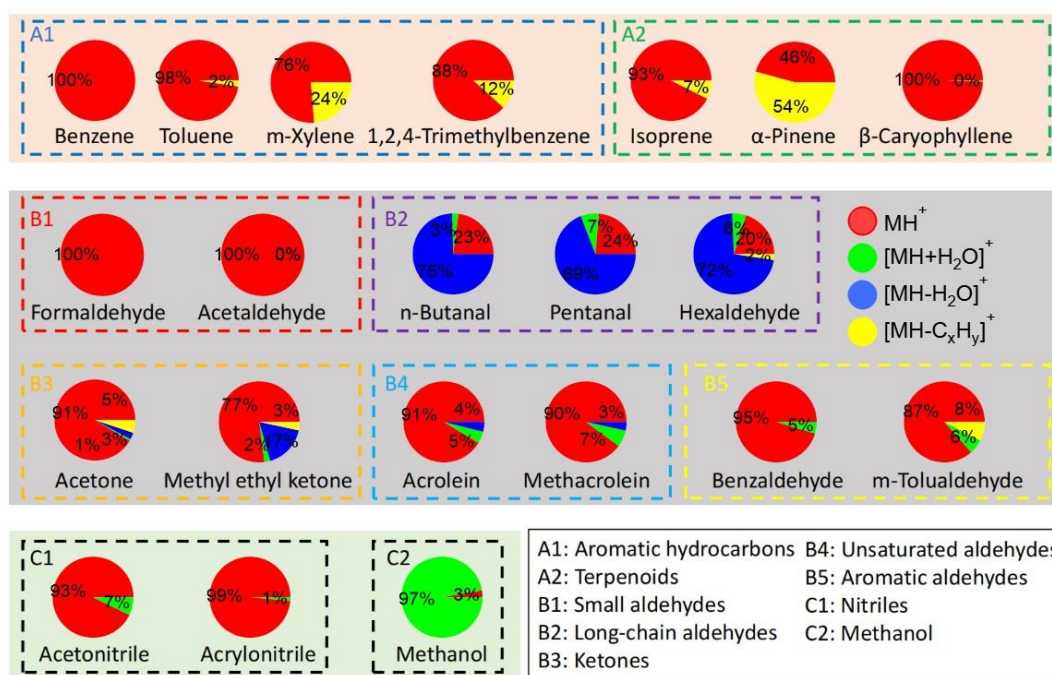
204
205 Figure 2. The average signal percentages of protonated, adduct, and fragmented ions

206 at a concentration of ~12 ppbv (~1.2 ppbv for β-caryophyllene).

207   For both dry and RH-dependent experiments, from the 1-minute averages from 1-

208 Hz datasets, the last five points were averaged to obtain stable signals. Figure S5 shows

209 the time series of selected hydrocarbons (groups A1 and A2, aromatic hydrocarbons

210 and terpenoids, Figure S5a) and OVOCs (groups B2 and B5, long-chain and aromatic

211 aldehydes, Figure S5b) during dry experiments with concentration stepping. Figure S6

212 shows the time series of protonated ions (MH^+), adduct ions ($[MH + H_2O]^+$), and

213 fragmented ions ($[MH - H_2O]^+$ and/or $[MH - C_xH_y]^+$ for n-butanal, pentanal and

214 hexaldehyde, whose adduct and fragmented ions contributed substantially to the total

215 signals (Figure 2 and Table S4). Some dealkylated fragments ($[MH - C_xH_y]^+$) of long-

216 chain aldehydes (e.g., n-butanal and pentanal) might overlap with the protonated ions

217 ($[MH]^+$) of unsaturated aldehydes (i.e., acrolein and methacrolein). Yet since the

218 intensities of the former are expected to be low by analogy with that of hexaldehyde

219 (~2%, Figure 2), the ions at those m/Q values are only considered as the protonated ions

220 of unsaturated aldehydes (the latter).

221   Similar to RH-dependent experiments, the duration of each instrument setting

222 experiment was 15 min. The signal intensities and the ratio of MH^+, $[MH + H_2O]^+$ and

223 $[MH - H_2O]^+$ and/or $[MH - C_xH_y]^+$ to all for two typical hydrocarbons (α-pinene and

224 1,2,4-trimethylbenzene) and two OVOCs (acetone and hexaldehyde) as the axial

225 voltage and pressure (which both affects the E/N ratio) in the FIMR, RF amplitude, and

226 BSQ amplitude varied are shown in Figures S7 to S10. The reduced electric field
227 parameter (E/N ratio) was estimated by comparing the signal fraction of fragment of α-
228 pinene in Materić et al. (2017), in which detailed examination on fragment signal
229 fraction at different E/N ratio was performed (Figure S11).

2.4 Sensitivity estimation

231 The formation of the protonated ion MH^+ via reaction R1 is desirable for
232 quantification of VOCs, which is described by the kinetics of the proton-transfer
233 reaction (de Gouw and Warneke, 2007;Yuan et al., 2017):

$$[MH^+] = [H_3O^+]_0 \ (1 - e^{-k[M]\Delta t}) \ \text{(Eq. 1)}$$

235 where $[MH^+]$ is the number concentration of the protonated ion, $[H_3O^+]_0$ that of the
236 initial hydronium ion, k is the rate constant of R1 (k_{ptr}), $[M]$ is the number concentration
237 of the target VOCs in the sample air, and Δt is the reaction time in the FIMR. Two
238 conditions allow simplification of Eq. 1 to Eq. 2 below for easy quantification of VOCs:
239 1) The term $k[M]\Delta t$ is much smaller than 1, such that R1 can be considered essentially
240 first-order; and 2) H_3O^+ is not significantly depleted and remain more or less constant
241 after the FIMR. Compared with traditional ion sources, the Vocus ion source produces
242 sufficient H_3O^+ (Krechmer et al., 2018). Ambient levels of ppbv (or less) for $[M]$ ($\sim 10^{10}$
243 molecule cm^{-3}) generally fulfill such requirements, given that k_{ptr} is on the order of 10^{-9} cm^3 molecule^{-1} s^{-1} and Δt of 10^{-4} s (Ellis and Mayhew, 2014). Therefore,

$$[MH^+] = [H_3O^+]k[M]\Delta t \ \text{(Eq. 2)}$$

246 where $[H_3O^+]$ is the mixing ratio of hydronium ions after the FIMR (i.e., being detected
247 in the mass spectrometer). Then,

$$[M] = \frac{I_{MH^+}}{I_{H_3O^+}} \frac{1}{k\Delta t} \ \text{(Eq. 3)}$$

249 where I_{MH^+} and I_{H3O^+} are signal intensities of the protonated ion and the hydronium ion,
250 respectively.
251 In general, the sensitivity (S) of PTR-MS for quantification of VOCs is defined as
252 the ratio between the signal intensity I_{MH^+} normalized by 10^6 cps (counts per second) of
253 I_{H3O^+} and 1 ppbv (10^{-9} mol mol^{-1}) of VOCs, i.e.:

254
$$S = \frac{\frac{I_{MH^+}}{I_{H_3O^+}} \times 10^6}{\frac{[M]}{N} \times 10^9} \quad \text{(Eq. 4)}$$

255 where N is the number density of air in the FIMR. The sensitivity S is thus expressed

256 as a normalized signal per ppbv, having a unit of ncps ppbv^{-1}. Combining Eq. 3 and Eq.

257 4 yields,

258
$$S = 10^{-3} \times N\Delta t \times k \, \text{(Eq. 5)}$$

259 where $10^{-3} \times N \Delta t$ is specific to the instrumental settings. Eq. 5 dictates that S should

260 have a linear relationship with the proton-transfer reaction rate constant (k_{ptr}) if the

261 instrument settings are fixed and can be utilized to predict S if k_{ptr} values are known

262 (Ellis and Mayhew, 2014).

263   In reality, however, quantification of VOCs using MH^+ from PTR-MS

264 measurements is complicated by 1) formation of adduct (e.g., with H_2O) and

265 fragmented (e.g., dehydration) ions, and 2) discriminated transmission for MH^+ ions

266 with different m/Q values (de Gouw and Warneke, 2007;Yuan et al., 2017). The fraction

267 of MH^+ in all related ions (f_{MH^+}) and the relative transmission efficiency (T_{MH^+}/T_{H3O^+})

268 are used to account for these two effects, respectively:

269
$$S = 10^{-3} \times N\Delta t \times \frac{T_{MH^+}}{T_{H_3O^+}} \times f_{MH^+} \times k \, \text{(Eq. 6)}$$

270   In our study, the sensitivity is expressed as the slope of signal intensity (in counts

271 per second, cps) vs. concentration (in ppbv), having a unit of cps ppbv^{-1} (Figure S12).

272 Signal normalization to H_3O^+ (ncps) was not adopted because the signal of H_3O^+ (m/Q

273 = 19 Th) was substantially suppressed with low transmission (see below) for those ions

274 with small m/Q values (but too high intensities) to minimize ion currents.

3 Results and Discussion

3.1 Effects of instrumental settings on the ion signals

277   An increase of the E/N ratio from 48 to 142 Td manifested by the increases of the

278 FIMR axial voltage (V, with front from 226 to 666 volts and back keeps at 34 volts) led

279 to drastic increases of MH^+ signal intensity by three to four orders of magnitude for all

280 VOCs studied (Figure 3a). Such increases were also observed for adduct and

fragmented ions (Figures S7 - S10), albeit to different extents. It has been shown that increasing the axial voltage in the FIMR can substantially increase protonated ion signals, which is due mainly to three reasons (Krechmer et al., 2018;de Gouw and Warneke, 2007). First, a high FIMR axial voltage can accelerate the ions and thus reduce their residence time, thereby preventing diffusional loss. Second, the high voltage in FIMR significantly increases the concentration of all reagent ions (Figure S13). Lastly, at high voltage, reactions between some OVOCs (such as acetone) and H_3O^+ leads to more protonated ions (MH^+) instead of adduct ions ($[MH + H_2O]^+$) through ligand switching reaction (R2b). The last effect was believed to be less significant for species that do not readily react with $H_3O^+(H_2O)_n$ (such as aromatics and terpenoids).
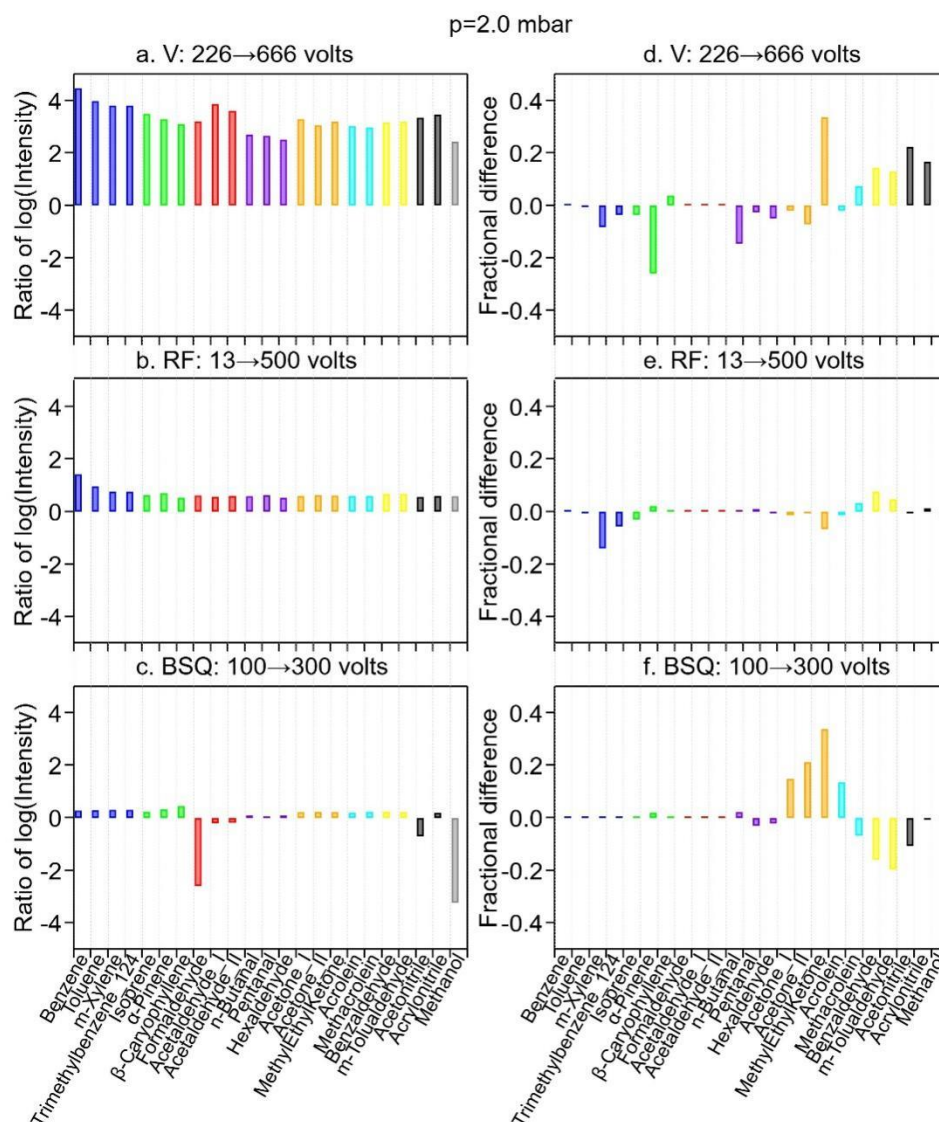
Figure 3. The ratio of the logarithm of intensity (panels a, b, and c) and the difference of fractional signal of the protonated ion (MH^+) among all ions (panels d, e, and f), when changing axial voltage (V) or FIMR pressure (p) (panels a and d), RF amplitude (panels b and e), and BSQ amplitude (panels c and f). The ratios were taken after taking the logarithm of the signal intensities of MH^+ at the right-hand side of the instrument setting (after the arrow) to that at the left-hand side of the instrument setting stated in the panel label; likewise, the fractional differences are the fractions of the MH^+ signal among the protonated, fragmented, and adduct signals under these two instrumental settings.

To investigate whether the desired MH^+ is indeed more favorably formed by suppressing R2b under high axial voltages, we plot the differences in the signal fractions of MH^+ between axial voltages of 666 volts and 226 volts (Figure 3d). The results show that about one-third of the 21 VOCs do not have significant differences in the signal fractions: most VOCs in this one-third have the MH^+ as the sole or dominating ion observed (*cf.*, Figure 2). Meanwhile, there are about one-third showing negative differences (i.e., decreasing MH^+ fractions) of up to 0.2, including the two hydrocarbons and two OVOCs shown in panel d of Figures S7 – S10. The remaining one-third show positive differences (i.e., increasing MH^+ fractions) of up to 0.3, mainly for unsaturated or aromatic aldehydes, as well as nitriles (Figure 3d). A closer inspection of the fractional changes as axial voltage increases for acetone (Figure S9d) and hexaldehyde (Figure S10d) reveals that the fractions of both MH^+ and $[MH + H_2O]^+$ decrease, while those of fragmented ions ($[MH – H_2O]^+$ and/or $[MH – C_xH_y]^+$) increase. The relative decreases of the signal fractions of MH^+ (8% for acetone and 51% for hexaldehyde) are, however, much lower than those of $[MH + H_2O]^+$ (57% for acetone and 80% for hexaldehyde). These observations suggest that while fractions of both MH^+ and $[MH + H_2O]^+$ decrease, the decreases of the adduct ion ($[MH + H_2O]^+$) are more significant, supporting the third reason that relatively more H_3O^+ (instead of $H_3O^+(H_2O)_n$) at higher axial voltages to react with these OVOCs. However, as the voltage increases, all ion signals are increasing (Figure S7a-S10a). This observation illustrates that the ion acceleration and diffusion prevention should be the primary reason for signal enhancement at high axial voltages. Nevertheless, the signal fractions of the MH^+ do not change substantially (within 30%) as the FIMR axial voltage increases, making quantification reliable even for species with high signal contributions from adduct and fragmented ions (e.g., long-chain aldehydes, group B2, *cf.*, Figure 2).

The increase of E/N ratio by decreasing FIMR pressure from 3.5 to 1.5 mbar increases signal intensities (Figure S14a) of MH^+ by less than one order of magnitude, or even decreases those for some OVOCs such as long-chain aldehydes. The changes in signal fractions of MH^+ (Figure S14d), on the other hand, are more than those when changing axial voltages, especially for ketones, unsaturated aldehydes, aromatic aldehydes, and nitriles. The increase of pressure in the PTR reactor also favors the formation of reagent clusters $H_3O^+(H_2O)_n$, which leads to the formation of adduct ions (Wang et al., 2020). For OVOCs acetone and hexaldehyde, the fractions of MH^+ do

increase when FIMR pressure was decreased from 3.5 to 2.5 mbar (E/N ratio from 162

to 95), which is accompanied by significant decreases of the adduct ion $[MH + H_2O]^+$

(Figure S9j and Figure S10j). This observation suggests less formation of adduct ions

at lower FIMR pressures. Further decrease of FIMR pressure to 1.5 mbar, however,

results in slight decreases of MH^+ fractions, in lieu of increases of fragmented ions [MH

$- H_2O]^+$ and $[MH - C_xH_y]^+$ (Figure S9j and Figure S10j); for hydrocarbons α-pinene

and 1,2,4-trimethylbenzene (Figure S7j and Figure S8j) that only have MH^+ and [MH

$- C_xH_y]^+$, continuous decreases of MH^+ fractions and increases of $[MH - C_xH_y]^+$ are

observed for the whole range of FIMR pressure tested (3.5 to 1.5 mbar). A recent study

using Vocus PTR-MS to measure organic peroxides also observed that less fragmented

ions were formed under higher FIMR pressure (Li et al., 2022), presumably due to the

efficient transfer of excess kinetic energy by frequent collisions at higher pressures. A

medium FIMR pressure of 2.0 mbar was chosen to have relatively low fractions of both

adduct ions ($[MH + H_2O]^+$) and fragmented ions ($[MH - H_2O]^+$ and $[MH - C_xH_y]^+$).

The radial RF electric field in the FIMR is unique for the Vocus PTR-MS, which

can (1) collimate the ions towards the central axis (especially heavier ions) and (2)

increase the kinetic energy of the ions (especially for lighter ions) (Krechmer et al.,

2018). These effects led to 1 to 1.5 orders of magnitude higher signals for MH^+ at 2.0

mbar FIMR pressure (Figure 3b) and 1.5 to 2 orders of magnitude at 3.5 mbar (Figure

S14b) when the RF amplitude was changed from 13 to 500 volts. The additional

enhancement of signal intensity at a higher FIMR pressure (i.e., 3.5 mbar as compared

to 2.0 mbar) can be attributed to a longer residence time of the reagent ions (Krechmer

et al., 2018). The more pronounced increase of kinetic energy for lighter ions (e.g.,

H_3O^+) than heavier ions [i.e., clusters $H_3O^+(H_2O)_n$] might imply the favorable

formation of the protonated ion MH^+ rather than adduct ions. The fractions of MH^+ for

different RF amplitudes do not change significantly (within ±0.2) either at 2.0 mbar

(Figure 3e) or 3.5 mbar (Figure S14e). This observation thus suggests that adding the

RF can increase signal intensities by $1 - 2$ orders of magnitude but does not affect the

fractional signal for MH^+, making it beneficial for accurate quantification.

The BSQ amplitude above 100 volts does not change the signal intensities

significantly (Figure 3c and Figure S14c, as well as Figures S7– S10). The BSQ ion

guide provides a high-pass band filter to reduce the number of ions (thus signal intensity)

of low m/Q values (especially for reagent ions, H_3O^+, with high ion currents),

368   preventing the fast degradation of the microchannel plate (MCP) detector (Krechmer et

369   al., 2018). This bandpass filter leads to lower ion transmission efficiency (<1) for ions

370   with smaller m/Q values, which is discussed below. Therefore, the signal reduction

371   when the BSQ amplitude increased from 100 to 300 volts is more obvious for small

372   analytes such as formaldehyde, acetonitrile, and methanol (Figure 3c and Figure S14c).

373   For other analytes whose fragmented ions have m/Q values of less than 60 Th, the signal

374   fractions of MH^+ would also be affected (Figure 3f and Figure S14f). For example, the

375   intensities of fragmented ions $[MH – H_2O]^+$ ($CH_3CCH_2^+$, $m/Q = 41$ Th) and $[MH –$

376   $C_xH_y]^+$ (CH_3CO^+, $m/Q = 43$ Th) for acetone had substantial decreases when BSQ

377   amplitude was higher than 200 volts (Figure S9c and Figure S10). The protonated ion

378   MH^+ ($CH_3COCH_3H^+$, $m/Q = 59$ Th) and adduct ion ($CH_3COCH_3H_3O^+$, $m/Q = 77$ Th),

379   however, remained less unaffected. This effect leads to noticeable changes in signal

380   fractions of MH^+ (maximum 0.4) for small analytes such as ketones, unsaturated

381   aldehydes, nitriles, as well as methanol (Figure 3f and Figure S14f) as the BSQ

382   amplitude changes from 100 to 300 volts.

383   **3.2 Sensitivity and transmission of protonated ions**

384   We calculated the sensitivity and transmission of protonated ions (MH^+) of the 21

385   VOCs studied when the instrument was under the optimized conditions. Table 1 shows

386   the sensitivities (cps ppbv^{-1}), as slopes of MH^+ signals vs. mixing ratios (average value

387   from 0 to 22 ppbv at dry condition, except for β-caryophyllene to 2 ppbv) and the limit

388   of detection (LOD, 3σ). Panels a and b in Figure 4 show the sensitivity vs. k_{ptr} for all

389   21 VOCs, while panels c and d show the transmission efficiencies calculated from the

390   division of the sensitivity vs. k_{ptr} ratio for each VOC by the slope fitted in Figure 4a and

391   4b.

392   Most VOCs had sensitivities above 1000 cps ppbv^{-1}, except 1) formaldehyde (A2-

393   1) and methanol (C2-1), whose MH^+ ions have m/Q values much lower than 60 Th; and

394   2) β-caryophyllene (A2-3) that came with a very low concentration range. In addition

395   to its low m/Q values that limit the transmission, the backward reaction is also an

396   important reason for the low sensitivity. For instance, formaldehyde has a low PA value

397   (712.5 kJ mol^{-1}) that is not much higher than that of water (691.0 kJ mol^{-1}) and has been

398   shown to have a high tendency of backward reaction of R1 (Inomata et al.,

399   2008;Vlasenko et al., 2010;Warneke et al., 2011). The two compounds in group B5

400 (aromatic aldehydes), benzaldehyde and m-tolualdehyde, had the highest sensitivities

401 of >12000 cps ppbv^{-1}. This might be due to their high PA values (>830 kJ mol^{-1}), which

402 are among the highest except those of terpenoids (Table S2).

403 Table 1. Sensitivity (slope), intercept, and limit of detection (LOD) based on 3 standard

404 deviations (σ) and cylinder numbers (No.). Results were obtained from measurements

405 of 0 – 22 ppbv for all VOCs except for β-caryophyllene (up to ~2 ppbv). The cylinder

406 numbers for the VOCs studied are also shown here.

Group[a]	Name	Cylinder No.	Label	Sensitivity (cps ppbv^{-1})	3σ LOD (pptv), 5 s
A1	Benzene	I	A1-1	2596	35
	Toluene	I	A1-2	5724	2
	m-Xylene	I	A1-3	8669	3
	1,2,4-Trimethylbenzene	I	A1-4	8951	1
A2	Isoprene	I	A2-1	2140	16
	α-Pinene	I	A2-2	4046	2
	β-Caryophyllene	I	A2-3	723	1
B1	Formaldehyde	II	B1-1	—[c]	—[c]
	Acetaldehyde	I&II	B1-2	2096[b]	283
B2	n-Butanal	II	B2-1	1114	343
	Pentanal	II	B2-2	1465	63
	Hexaldehyde	II	B2-3	1595	35
B3	Acetone	I&II	B3-1	9932[b]	127
	Methyl ethyl ketone	I	B3-3	9636	51
B4	Acrolein	I	B4-1	7224	16
	Methacrolein	I	B4-2	6090	13
B5	Benzaldehyde	II	B5-1	16089	1
	m-Tolualdehyde	II	B5-2	12893	1
C1	Acetonitrile	I	C1-1	1511	6
	Acrylonitrile	I	C1-2	9275	1
C2	Methanol	I	C2-1	—[c]	—[c]

407 Notes:
408 a, A1: aromatic hydrocarbons, A2: terpenoids, B1: small aldehydes; B2: long-chain aldehydes, B3:
409 ketones, B4: unsaturated aldehydes, B5: aromatic aldehydes, C1: nitriles, C2: methanol;
410 b, the average value from gas cylinders I and II, with a deviation of less than ±1.5%.;
411 c, low sensitivity and high LOD due to low transmission.
412
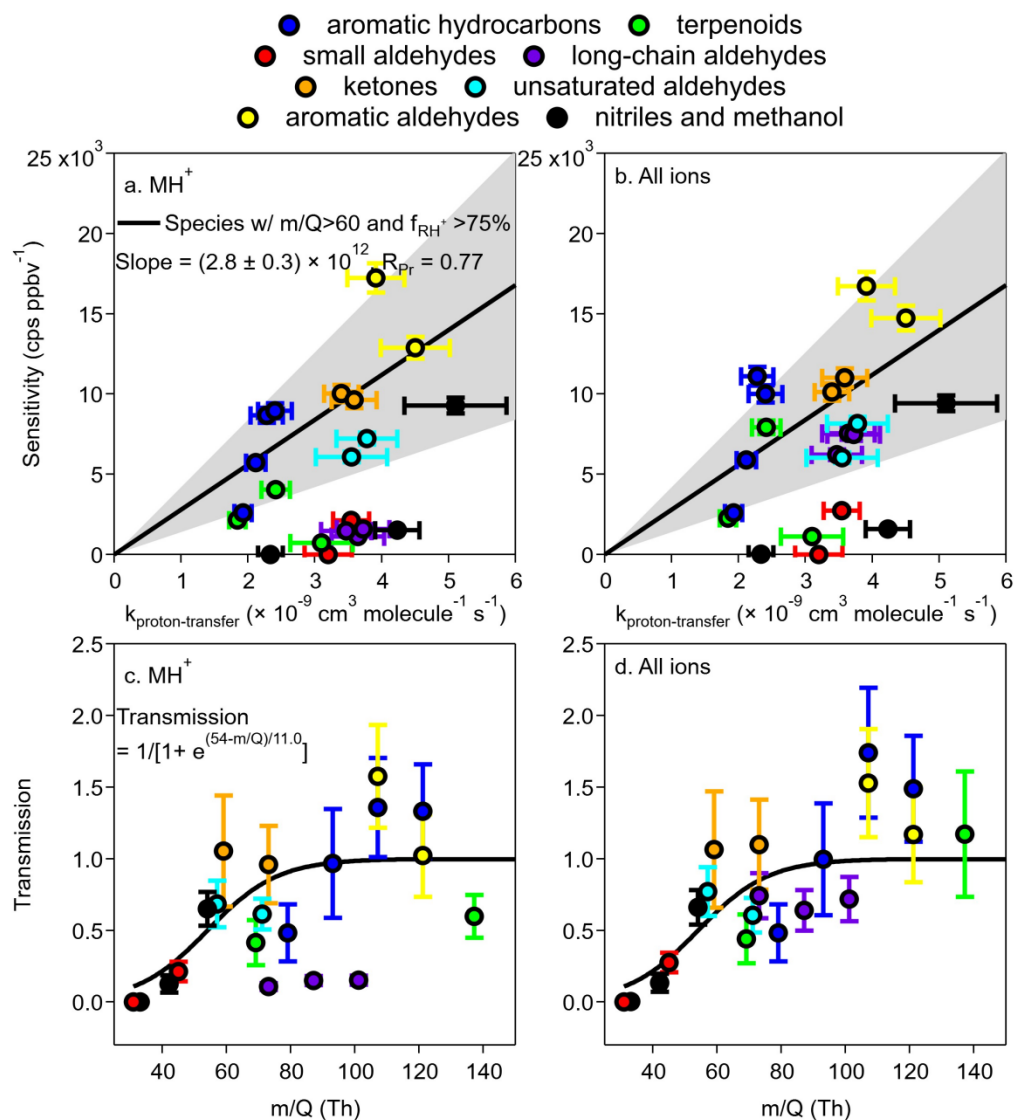
413
414 Figure 4. Sensitivity as a function of k_{ptr} for (a) MH[+] and (b) all ions. Linear fitting was

415 performed only for MH[+] sensitivity. Species included in the fitting were those with m/Q

416 value > 60 Th (Table S2) and signal percentage of MH[+] (f_{MH^+}) > 75% (Table 1). The

417 grey-shaded area is bounded by $0.5 \times$ Slope and $2 \times$ Slope. The fitted curves in panel b

418 are the same as in panel a and are for reference only. Panels c and d are transmission

419 curves from MH[+] only and from the sum of all ions, respectively. The sigmoidal curve

420 for MH[+] (same for c and d) was fitted from species except for β-caryophyllene, α-pinene,

421 n-butanal, pentanal, and hexaldehyde whose fragmentation was significant. Note that

422 only the m/Q values of MH[+] was used in the x axes of panel c and d, although panel d

423 contains information of adduct and fragmented ions that have m/Q values different from

424 that of MH[+], which does not consider the differences in m/Q values of adduct and

425 fragmented ions.

426   It was shown that the sensitivities for different VOCs in PTR-MS can be calculated

427   from the kinetics of the proton-transfer reactions (Warneke et al., 2003;Sekimoto et al.,

428   2017;Cappellin et al., 2012). For Vocus, Krechmer et al. (2018) also pointed out that

429   the relationship between sensitivity and k_{ptr} can be established and used to calculate the

430   sensitivity for other compounds. We herein compare the relationship between

431   sensitivity and k_{ptr} (Figure 4a). In our data, the uncertainties for sensitivity were

432   conservatively taken as the maximum percentage uncertainty (5.3%) of fitted slopes.

433   Values of k_{ptr} were calculated as averages of both modeled and experimental results

434   found from literature (Table S3), with uncertainties propagated from an estimated

435   percentage error of 15% for both modeled (Zhao and Zhang, 2004) and experimental

436   values. The anticipated linear relationship of sensitivity vs. k_{ptr} is not easily visible,

437   most likely due to the formation of fragments/adducts for some VOCs and low

438   transmission efficiencies for others. However, a relatively improved linear relationship

439   was found if we limit the VOCs to 1) m/Q values for MH^+ > 60 Th, and 2) a fraction of

440   MH^+ ion in all ions (including adduct/fragmented ions) larger than 75% (*cf*, Figure 2).

441   With these limitations, the fitted linear line gives a slope of $(2.8 \pm 0.3) \times 10^{12}$ cps ppbv^{-1}

442   ^{1} molec s cm^{-3}, approximately 38% lower than that $[(4.5 \pm 0.4) \times 10^{12}$ cps ppbv^{-1} molec

443   s cm^{-3}] of Krechmer et al. (2018). Pearson's R (R_{Pr}) is 0.77. A grey area is also shown

444   by two lines of 2 × slope and 0.5 × slope, which includes approximately half (ten) of

445   the VOCs studied. Those that fall out of the grey area to the lower region are mainly

446   compounds in groups B2 (long-chain aldehydes, purple), C1 and C2 (nitriles or

447   methanol, black), B1 (small aldehydes, red), and A2 (terpenoids, green). Using the total

448   signals of all ions (protonated, adduct, and fragmented), Figure 4b shows the

449   improvements for compounds in group B2 only, while others (especially those in C1,

450   C2, and B1) do not move up to the grey area.

451   We also calculated the transmission efficiencies (Figure 4c and 4d) from the

452   division of the sensitivity vs. k_{ptr} ratio for each VOC by the slope fitted in Figure 4a. It

453   is shown that compounds in groups B1, C1, and C2 are mainly on the rising range of

454   the sigmoidal curve, while the three long-chain aldehydes in group B2 (purple) are well

455   below the curve if only MH^+ ions were used; these three long-chain aldehydes move up

456   to transmission > 0.5 when all ions are considered (Figure 4d). Of particular interest is

457   the compound α-pinene, whose transmission was < 0.5 when only the MH^+ ion was

458   used, but it increases to about 1.5 when the fragmented ion was considered. Note that

459 in Figure 4d, the m/Q value of MH$^+$ was used in the x axis for the summed ion signals,

460 which might lead to certain bias as the fragmented and adduct ions have different m/Q

461 values. Nevertheless, the above analysis suggests that both the formation of

462 adduct/fragmented ions and transmission affect the relationship between sensitivity and

463 k_{ptr}, which needs precaution when using predicted sensitivity directly from k_{ptr}. In

464 addition, one needs to be cautious about the prediction of transmission efficiency with

465 m/Q greater than 150.

3.3 RH dependence of ion signals

467 One of the most important reasons for RH dependence is that the distribution of

468 reagent ions might vary with ambient RH, especially when the abundance of H$_3$O$^+$ in

469 the PTR reactor is not high. While the Vocus has been shown to have abundant enough

470 H$_3$O$^+$ (Krechmer et al., 2018), whether it can substantially minimize RH dependence

471 for most VOCs deserves scrutinization. Figure 5a-h shows the relative sensitivity,

472 defined as the relative change of sensitivity of MH$^+$ ion vs. VOC concentration under

473 different RH conditions. Among the nine groups of VOCs studied, seven groups show

474 almost flat relative sensitivities within the RH range of ~5% to ~85% (298 K), with the

475 exceptions of long-chain aldehydes (group B2) that show increasing sensitivities as RH

476 increases (Figure 5d) and methanol (group C2) showing large variations (Figure 5h).

477 Some other compounds, such as β-caryophyllene (A2-3, Figure 5b) and formaldehyde

478 (B1-1, Figure 5c) also show either relatively large uncertainties or fluctuations, which

479 can be ascribed to their low intensities (*cf.*, Table 1).
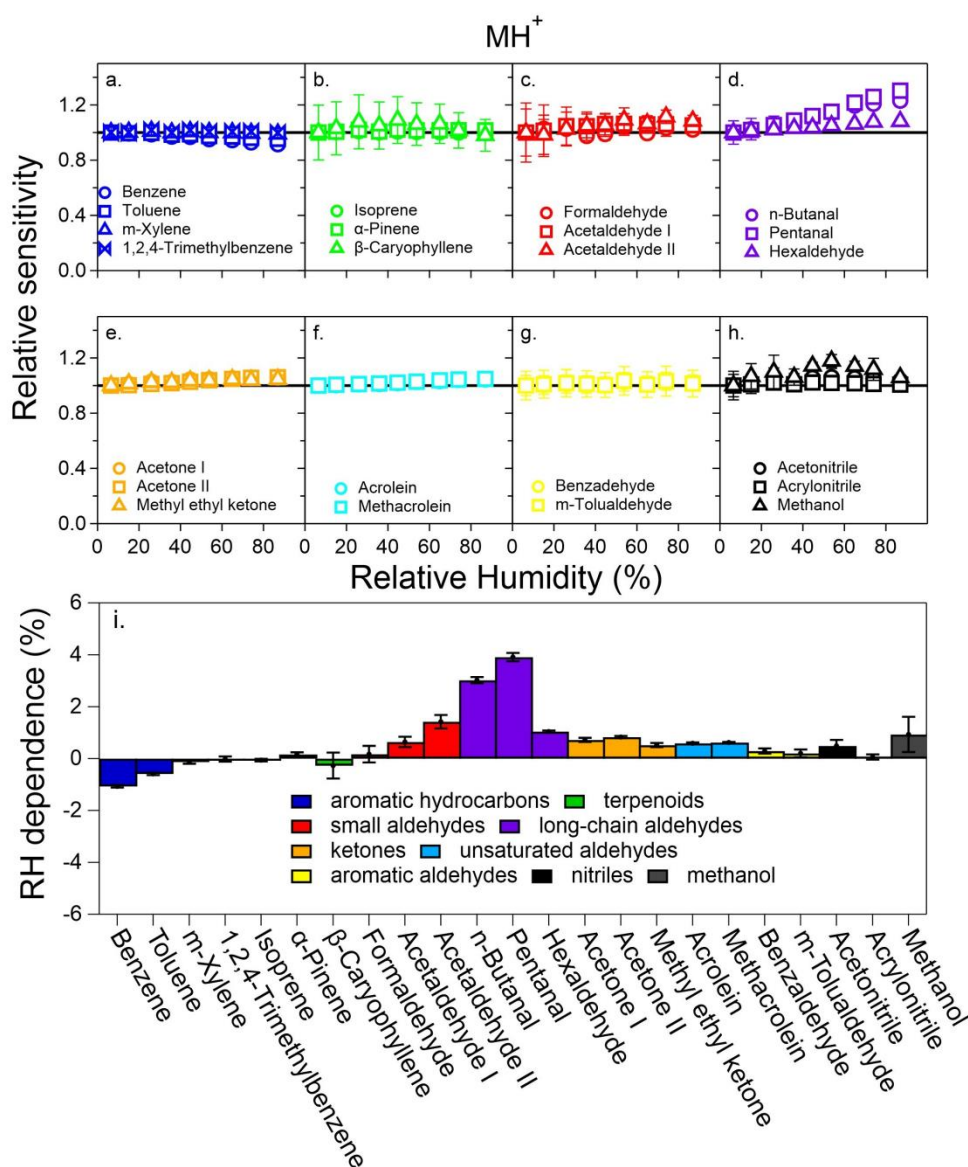
Figure 5. The dependence of the MH$^+$ signals on RH for the VOCs studied. Panels a-h: the relative sensitivity was calculated as the slope (Sensitivity) under all conditions to that at the dry (RH<5%) condition. Panel i: the percent change of relative sensitivity per 10% RH increase. See Figures S15-S17 for other ion signals.

Figure 5i shows the RH dependence of the MH$^+$ ions, defined as the percentage change of sensitivity per 10% RH increase, for all 21 VOCs studied. Aromatic hydrocarbons (group A1) show negative RH dependence as in previous studies using PTR-MS with a drift tube (Warneke et al., 2001;Steinbacher et al., 2004). While previous studies reported decreases in benzene sensitivity by 16 – 56% from dry to humid conditions (up to 100% RH), our results show a decrease of less than 1.1% per 10% RH increase (i.e., <11% in the whole RH range) with a somewhat narrower RH

range (up to ~85% RH). In addition, two out of the three terpenoids (group A2) also show slightly negative RH dependence, and the other one (α-pinene) shows very small positive RH dependence (Figure 5i). These hydrocarbons (aromatics and terpenoids) in groups A1 and A2 have relatively low k_{ptr} values (mostly $<2.5 \times 10^{-9}$ cm^3 $molec^{-1}$ s^{-1}, Table S3), and their RH dependence shows a fairly good correlation with the PA value (Figure 6a, purple circles and squares). This observation suggests that there might be a thermodynamic reason behind the noticeable decrease of sensitivity for hydrocarbons such as benzene as RH increases. Since hydrocarbons such as benzene and toluene do not readily react with $H_3O^+(H_2O)$ (Warneke et al., 2001), R1 is the main reaction to form MH^+. As water vapor concentration increases at high RH, the reverse reaction of R1 might be important for compounds with low PA and low k_{ptr} values (Inomata et al., 2008).
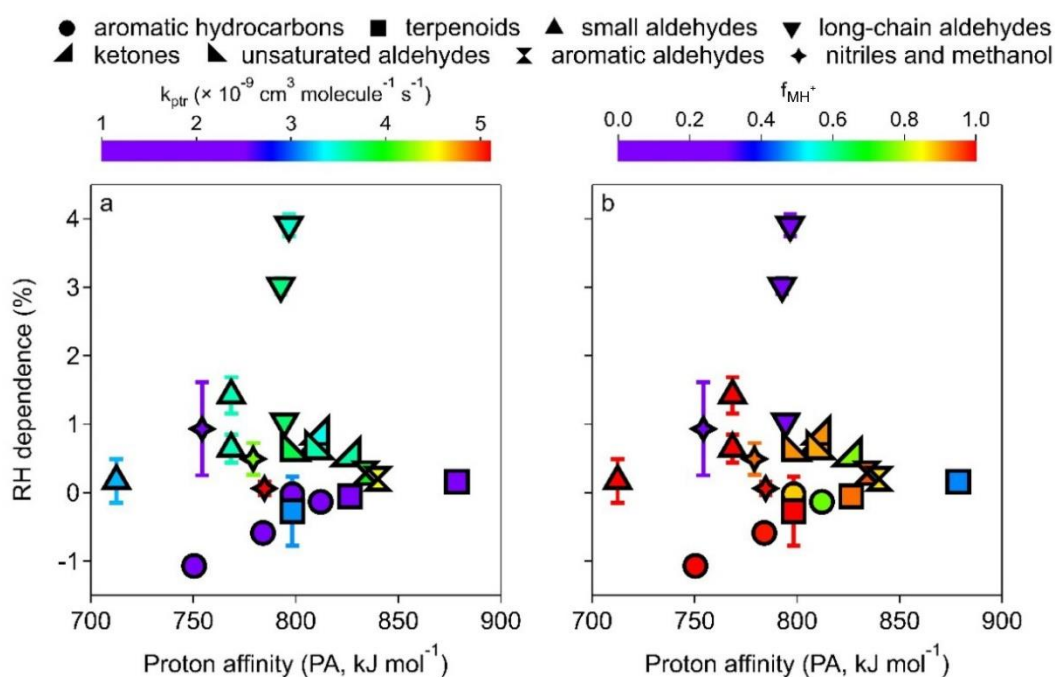
Figure 6: The RH dependence of MH^+ ion plotted against PA, color-coded by (a) k_{ptr} and (b) f_{MH^+}.

Long-chain aldehydes (group B2) have the largest RH dependence of 1-4% positive deviation per 10% RH increase for the MH^+ ions. The RH dependence of the $[MH + H_2O]^+$ ions (Figure S15g) is even much higher (1.4–8.5% positive deviation per 10% RH increase). Interestingly, the trends of RH dependence for the MH^+ ions and that for the $[MH + H_2O]^+$ ions for long-chain aldehydes are exactly opposite (Figure 5i

and Figure S15g); that is, pentanal > n-butanal > hexaldehyde. The reason behind this observation is out of the scope of this study. The dominating $[MH - H_2O]^+$ ions for long-chain aldehydes (Figure 2), however, show much less ($\pm$1% per 10% RH increase) RH dependence (Figure S16i). Other carbonyl compounds (groups B1, B3, B4, and B5) also show positive deviations as RH increases (less than 1.5% increase in sensitivity per 10% RH increase), albert to various degrees (Figure 5i). Similar to long-chain aldehydes, their $[MH + H_2O]^+$ ions also show a large positive deviation (Figure S16g), and $[MH - H_2O]^+$ ions show little RH dependence (Figure S16e). These carbonyl compounds have medium PA values (Figure 6a) except formaldehyde. If we exclude formaldehyde (with an extremely low PA value, the up triangle to the far left in Figure 6b) and long-chain aldehydes (low percentages of MH^+ ions, <25%, down triangles in Figure 6b), the RH dependence of other carbonyl compounds shows a slightly decreasing trend of RH dependence vs. PA values (Figure 6b, up triangles, left triangles, right triangles, and double triangles). These observations might hint on the relationships between the RH dependence of carbonyl compounds and reagent ion distribution as well as reaction direction for R1-R4, which is different from those for pure hydrocarbons (groups A1 and A2). Finally, the RH dependence of MH^+ for compounds in groups C1 (nitriles) and C2 (methanol) is within +1% per 10% RH increase (Figure 5i).

Overall, in the whole RH range studied (~5% to ~85%), the RH dependence of MH^+ ions for the 21 VOCs studied is less than 30%, with most compounds (except group B2, long-chain aldehydes) less than 15%. For $[MH + H_2O]^+$ ions (mainly for carbonyl compounds), strong RH dependence was observed (Figure S15), being 1.4 – 8.5% per 10% RH increase, or 8.9 – 63.2% from ~5% to ~85% RH. The dehydrated ions ($[MH - H_2O]^+$), however, show the smallest RH dependence ($\pm$1% per 10% RH increase) among all the ions (Figure S16). Fragmented ions with decarbonization ($[MH - C_xH_y]^+$) show mainly negative RH dependence, generally less than 3% per 10% RH increase (Figure S17).

4 Conclusions

We investigated the response of protonated, adduct, and fragmented ions of 21 atmospherically relevant VOCs in a Vocus PTR-MS as instrument setting and RH condition vary. For the two ways of increasing the E/N ratio, increasing the FIMR axial

voltage can substantially (by three to four orders of magnitude) increase sensitivity but does not change the fractions of the MH^+ ions (mostly within 30%); reducing the FIMR pressure, however, does not enhance sensitivity much but can lead to more substantial fragmentation. Therefore, a high FIMR axial voltage of 600 – 700 volts and a medium pressure of around 2.0 mbar are recommended. Increasing the RF amplitude of FIMR can increase sensitivity by 1 to 1.5 orders of magnitude at 2.0 mbar and 1.5 to 2 orders of magnitude at 3.5 mbar, and it does not change the MH^+ ion fractions (within 20%). Therefore, a high RF amplitude of 500 V is recommended. Increasing the BSQ amplitude does not increase the sensitivity much but changes the MH^+ ion fractions of small ions substantially by changing the transmission efficiency. The choice of this instrument setting mainly relies on what ions (i.e., those reagent ions with too high an abundance) one wants to filter out. Our choice is at 300 V, which gives a 50% transmission at about 55 Th.

The relationship between sensitivity and k_{ptr} is strongly affected by two factors: 1) whether the MH^+ ion has a high transmission efficiency, and 2) whether the MH^+ ion is the dominating ion. If so, a fairly good correlation ($R_{Pr} = 0.77$) was observed for the VOCs studied. The transmission curve is also more reasonably resembling the sigmoid function only if all the ions (protonated, adduct, and fragmented) are considered. The low transmission efficiencies of formaldehyde and methanol result in extremely low sensitivities of these two small OVOCs, although a low PA value is another reason for the former.

As RH increases from ~5% to ~85%, the MH^+ ions for 19 out of the 21 VOCs studied have sensitivity variation of less than 15%, but long-chain aldehydes have positive RH dependence of up to 30%. The RH dependence of $[MH + H_2O]^+$ ions for long-chain aldehydes is stronger, while that of the dominating $[MH - H_2O]^+$ ions is limited. Therefore, the signal distributions among protonated, adduct, and fragmented ions are also affected by RH variation. Together with their relatively high background signals (especially for n-butanal, Figure S5b), quantification of long-chain aldehydes in the ambient environment using Vocus requires special attention. It is also worth noting that hydrocarbons generally show slight negative RH dependence, probably due to their relatively low k_{ptr} values, although such RH dependence does not affect quantification significantly; their RH dependence has a fairly good correlation with their PA values, hinting a thermodynamic reason behind this trend.

577

Competing interests

At least one of the (co-)authors is a member of the editorial board of Atmospheric Measurement Techniques.

Acknowledgments

This work was supported by funding support from the Science and Technology Development Fund, Macau SAR (File No. FDCT 0031/2023/AFJ) and a multiyear research grant (No. MYRG2022-00027-FST) from the University of Macau.

585

References

Baasandorj, M., Millet, D. B., Hu, L., Mitroo, D., and Williams, B. J.: Measuring acetic and formic acid by proton-transfer-reaction mass spectrometry: sensitivity, humidity dependence, and quantifying interferences, Atmos. Meas. Tech., 8, 1303-1321, https://doi.org/10.5194/amt-8-1303-2015, 2015.

Cappellin, L., Karl, T., Probst, M., Ismailova, O., Winkler, P. M., Soukoulis, C., Aprea, E., Märk, T. D., Gasperi, F., and Biasioli, F.: On Quantitative Determination of Volatile Organic Compound Concentrations Using Proton Transfer Reaction Time-of-Flight Mass Spectrometry, Environmental Science & Technology, 46, 2283-2290, https://doi.org/10.1021/es203985t, 2012.

Claflin, M. S., Pagonis, D., Finewax, Z., Handschy, A. V., Day, D. A., Brown, W. L., Jayne, J. T., Worsnop, D. R., Jimenez, J. L., Ziemann, P. J., de Gouw, J., and Lerner, B. M.: An in situ gas chromatograph with automatic detector switching between PTR- and EI-TOF-MS: isomer-resolved measurements of indoor air, Atmospheric Measurement Techniques 14, 133-152, https://doi.org/10.5194/amt-14-133-2021, 2021.

Cui, L., Zhang, Z., Huang, Y., Lee, S. C., Blake, D. R., Ho, K. F., Wang, B., Gao, Y., Wang, X. M., and Louie, P. K. K.: Measuring OVOCs and VOCs by PTR-MS in an urban roadside microenvironment of Hong Kong: relative humidity and temperature dependence, and field intercomparisons, Atmos. Meas. Tech., 9, 5763-5779, https://doi.org/10.5194/amt-9-5763-2016, 2016.

de Gouw, J., and Warneke, C.: Measurements of volatile organic compounds in the earths atmosphere using proton-transfer-reaction mass spectrometry, Mass Spectrom Rev, 26, 223-257, https://doi.org/10.1002/mas.20119, 2007.

de Gouw, J. A., Goldan, P. D., Warneke, C., Kuster, W. C., Roberts, J. M., Marchewka, M., Bertman, S. B., Pszenny, A. A. P., and Keene, W. C.: Validation of proton transfer reaction-mass spectrometry (PTR-MS) measurements of gas-phase organic compounds in the atmosphere during the New England Air Quality Study (NEAQS) in 2002, Journal of Geophysical Research: Atmospheres, 108, https://doi.org/10.1029/2003JD003863, 2003.

Ellis, A. M., and Mayhew, C. A.: Chemical Ionization: Chemistry, Thermodynamics and Kinetics, in: Proton Transfer Reaction Mass Spectrometry, 25-48, 2014.

Gueneron, M., Erickson, M. H., VanderSchelden, G. S., and Jobson, B. T.: PTR-MS fragmentation patterns of gasoline hydrocarbons, International Journal of Mass Spectrometry, 379, 97-109, https://doi.org/10.1016/j.ijms.2015.01.001, 2015.

Hansel, A., Jordan, A., Holzinger, R., Prazeller, P., Vogel, W., and Lindinger, W.: Proton transfer reaction mass spectrometry: on-line trace gas analysis at the ppb level, International Journal of Mass Spectrometry and Ion Processes, 149-150, 609-619, https://doi.org/10.1016/0168-1176(95)04294-U, 1995.

Hartungen, E. v., Wisthaler, A., Mikoviny, T., Jaksch, D., Boscaini, E., Dunphy, P. J., and Märk, T. D.: Proton-transfer-reaction mass spectrometry (PTR-MS) of carboxylic acids: Determination of Henry's law constants and axillary odour investigations, International Journal of Mass Spectrometry, 239, 243-248, https://doi.org/10.1016/j.ijms.2004.09.009, 2004.

Inomata, S., Tanimoto, H., Kameyama, S., Tsunogai, U., Irie, H., Kanaya, Y., and Wang, Z.: Technical Note: Determination of formaldehyde mixing ratios in air with PTR-MS: laboratory experiments and field measurements, Atmospheric Chemistry and Physics, 8, 273-284, https://doi.org/10.5194/acp-8-273-2008, 2008.

Jensen, A., Liu, Z., Tan, W., Dix, B., Chen, T., Koss, A., Zhu, L., Li, L., and de Gouw, J.: Measurements of Volatile Organic Compounds During the COVID-19 Lockdown in Changzhou, China, Geophysical Research Letters, 48, e2021GL095560, https://doi.org/10.1029/2021GL095560, 2021.

Kari, E., Miettinen, P., Yli-Pirilä, P., Virtanen, A., and Faiola, C. L.: PTR-ToF-MS product ion distributions and humidity-dependence of biogenic volatile organic compounds, International Journal of Mass Spectrometry, 430, 87-97, https://doi.org/10.1016/j.ijms.2018.05.003, 2018.

Krechmer, J., Lopez-Hilfiker, F., Koss, A., Hutterli, M., Stoermer, C., Deming, B., Kimmel, J., Warneke, C., Holzinger, R., Jayne, J., Worsnop, D., Fuhrer, K., Gonin, M., and de Gouw, J.: Evaluation of a New Reagent-Ion Source and Focusing Ion–Molecule Reactor for Use in Proton-Transfer-Reaction Mass Spectrometry, Anal Chem, 90, 12011-12018, https://doi.org/10.1021/acs.analchem.8b02641, 2018.

Li, H., Almeida, T. G., Luo, Y., Zhao, J., Palm, B. B., Daub, C. D., Huang, W., Mohr, C., Krechmer, J. E., Kurtén, T., and Ehn, M.: Fragmentation inside proton-transfer-reaction-based mass spectrometers limits the detection of ROOR and ROOH peroxides, Atmos. Meas. Tech., 15, 1811-1827, https://doi.org/10.5194/amt-15-1811-2022, 2022.

Lindinger, W., Hansel, A., and Jordan, A.: On-line monitoring of volatile organic compounds at pptv levels by means of proton-transfer-reaction mass spectrometry (PTR-MS) medical applications, food control and environmental research, International Journal of Mass Spectrometry and Ion Processes, 173, 191-241, https://doi.org/10.1016/S0168-1176(97)00281-4, 1998.

Materić, D., Lanza, M., Sulzer, P., Herbig, J., Bruhn, D., Gauci, V., Mason, N., and & Turner, C.: Selective

reagent ion-time of flight-mass spectrometry study of six common monoterpenes, International Journal of Mass Spectrometry, 421, 40-50, https://doi.org/10.1016/j.ijms.2017.06.003, 2017.

Michoud, V., Sauvage, S., Léonardis, T., Fronval, I., Kukui, A., Locoge, N., and Dusanter, S.: Field measurements of methylglyoxal using proton transfer reaction time-of-flight mass spectrometry and comparison to the DNPH–HPLC–UV method, Atmospheric Measurement Techniques, 11, 5729-5740, https://doi.org/10.5194/amt-11-5729-2018, 2018.

Pagonis, D., Sekimoto, K., and de Gouw, J.: A Library of Proton-Transfer Reactions of H3O+ Ions Used for Trace Gas Detection, J Am Soc Mass Spectr, 30, 1330-1335, https://doi.org/10.1007/s13361-019-02209-3, 2019.

Pleil, J. D., Hansel, A., and Beauchamp, J.: Advances in proton transfer reaction mass spectrometry (PTR-MS): applications in exhaled breath analysis, food science, and atmospheric chemistry, J Breath Res, 13, https://doi.org/10.1088/1752-7163/ab21a7, 2019.

Salazar Gómez, J. I., Sojka, M., Klucken, C., Schlögl, R., and Ruland, H.: Determination of trace compounds and artifacts in nitrogen background measurements by proton transfer reaction time-of-flight mass spectrometry under dry and humid conditions, J Mass Spectrom, 56, e4777, https://doi.org/10.1002/jms.4777, 2021.

Schripp, T., Etienne, S., Fauck, C., Fuhrmann, F., Märk, L., and Salthammer, T.: Application of proton-transfer-reaction-mass-spectrometry for Indoor Air Quality research, Indoor Air, 24, 178-189, https://doi.org/10.1111/ina.12061, 2014.

Sekimoto, K., Li, S.-M., Yuan, B., Koss, A., Coggon, M., Warneke, C., and de Gouw, J.: Calculation of the sensitivity of proton-transfer-reaction mass spectrometry (PTR-MS) for organic trace gases using molecular properties, International Journal of Mass Spectrometry, 421, 71-94, https://doi.org/10.1016/j.ijms.2017.04.006, 2017.

Sekimoto, K., and Koss, A. R.: Modern mass spectrometry in atmospheric sciences: Measurement of volatile organic compounds in the troposphere using proton-transfer-reaction mass spectrometry, J Mass Spectrom, 56, https://doi.org/10.1002/jms.4619, 2021.

Shao, P., An, J., Xin, J., Wu, F., Wang, J., Ji, D., and Wang, Y.: Source apportionment of VOCs and the contribution to photochemical ozone formation during summer in the typical industrial area in the Yangtze River Delta, China, Atmospheric Research, 176-177, 64-74, https://doi.org/10.1016/j.atmosres.2016.02.015, 2016.

Shrivastava, M., Cappa, C. D., Fan, J., Goldstein, A. H., Guenther, A. B., Jimenez, J. L., Kuang, C., Laskin, A., Martin, S. T., Ng, N. L., Petaja, T., Pierce, J. R., Rasch, P. J., Roldin, P., Seinfeld, J. H., Shilling, J., Smith, J. N., Thornton, J. A., Volkamer, R., Wang, J., Worsnop, D. R., Zaveri, R. A., Zelenyuk, A., and Zhang, Q.: Recent advances in understanding secondary organic aerosol: Implications for global climate forcing, Reviews of Geophysics, 55, 509-559, https://doi.org/10.1002/2016RG000540, 2017.

Sinha, V., Custer, T. G., Kluepfel, T., and Williams, J.: The effect of relative humidity on the detection of pyrrole by PTR-MS for OH reactivity measurements, International Journal of Mass Spectrometry, 282, 108-111, https://doi.org/10.1016/j.ijms.2009.02.019, 2009.

Smith, D., Diskin, A., Ji, Y. F., and Spanel, P.: Concurrent use of H3O+, NO+, and O-2(+) precursor ions for the detection and quantification of diverse trace gases in the presence of air and breath by selected ion-flow tube mass spectrometry, INTERNATIONAL JOURNAL OF MASS SPECTROMETRY, 209, 81-97, https://doi.org/10.1016/S1387-3806(01)00478-X, 2001.

Španěl, P., and Smith, D.: SIFT studies of the reactions of H3O+, NO+ and O+2 with a series of volatile carboxylic acids and esters, International Journal of Mass Spectrometry and Ion Processes, 172, 137-147, https://doi.org/10.1016/S0168-1176(97)00246-2, 1998.

Španěl, P., and Smith, D.: Selected ion flow tube: a technique for quantitative trace gas analysis of air and breath, Medical and Biological Engineering and Computing, 34, 409-419, https://doi.org/10.1007/BF02523843, 1996.

Španěl, P., Ji, Y., and Smith, D.: SIFT studies of the reactions of H3O+, NO+ and O2+ with a series of aldehydes and ketones, International Journal of Mass Spectrometry and Ion Processes, 165-166, 25-37, https://doi.org/10.1016/S0168-1176(97)00166-3, 1997.

Španěl, P., and Smith, D.: Influence of water vapour on selected ion flow tube mass spectrometric analyses of trace gases in humid air and breath, Rapid Communications in Mass Spectrometry, 14, 1898-1906, https://doi.org/10.1002/1097-0231(20001030)14:20<1898::AID-RCM110>3.0.CO;2-G, 2000.

Steinbacher, M., Dommen, J., Ammann, C., Spirig, C., Neftel, A., and Prevot, A. S. H.: Performance characteristics of a proton-transfer-reaction mass spectrometer (PTR-MS) derived from laboratory and field measurements, International Journal of Mass Spectrometry, 239, 117-128, https://doi.org/10.1016/j.ijms.2004.07.015, 2004.

Vlasenko, A., Macdonald, A. M., Sjostedt, S. J., and Abbatt, J. P. D.: Formaldehyde measurements by Proton transfer reaction - Mass Spectrometry (PTR-MS): correction for humidity effects, Atmospheric

705 Measurement Techniques, 3, 1055-1062, https://doi.org/10.5194/amt-3-1055-2010, 2010.

706 Wang, Y., Yang, G., Lu, Y., Liu, Y., Chen, J., and Wang, L.: Detection of gaseous dimethylamine using
707 vocus proton-transfer-reaction time-of-flight mass spectrometry, Atmospheric Environment, 243, 117875,
708 https://doi.org/10.1016/j.atmosenv.2020.117875, 2020.

709 Warneke, C., van der Veen, C., Luxembourg, S., de Gouw, J. A., and Kok, A.: Measurements of benzene
710 and toluene in ambient air using proton-transfer-reaction mass spectrometry: calibration, humidity
711 dependence, and field intercomparison, International Journal of Mass Spectrometry, 207, 167-182,
712 https://doi.org/10.1016/S1387-3806(01)00366-9, 2001.

713 Warneke, C., De Gouw, J. A., Kuster, W. C., Goldan, P. D., and Fall, R.: Validation of atmospheric VOC
714 measurements by proton-transfer-reaction mass spectrometry using a gas-chromatographic preseparation
715 method, Environ Sci Technol, 37, 2494-2501, https://doi.org/10.1021/es026266i, 2003.

716 Warneke, C., Veres, P., Holloway, J. S., Stutz, J., Tsai, C., Alvarez, S., Rappenglueck, B., Fehsenfeld, F.
717 C., Graus, M., Gilman, J. B., and de Gouw, J. A.: Airborne formaldehyde measurements using PTR-MS:
718 calibration, humidity dependence, inter-comparison and initial results, Atmos. Meas. Tech., 4, 2345-2358,
719 https://doi.org/10.5194/amt-4-2345-2011, 2011.

720 Yuan, B., Koss, A. R., Warneke, C., Coggon, M., Sekimoto, K., and de Gouw, J. A.: Proton-Transfer-
721 Reaction Mass Spectrometry: Applications in Atmospheric Sciences, Chemical Reviews, 117, 13187-
722 13229, https://doi.org/10.1021/acs.chemrev.7b00325, 2017.

723 Zhao, J., and Zhang, R.: Proton transfer reaction rate constants between hydronium ion (H3O+) and
724 volatile organic compounds, Atmospheric Environment, 38, 2177-2185,
725 https://doi.org/10.1016/j.atmosenv.2004.01.019, 2004.

726